Parametric analysis of composite sinusoidal specimens under quasi-static crushing

H. L. Mou

X. Su, J. Xie and Z. Y. Feng
caucstructure@163.com
Key Laboratory of Civil Aircraft Airworthiness Technology
Civil Aviation University of China
Tianjin
China

ABSTRACT

This paper aims to build the finite element model of the composite sinusoidal specimens and to carry out the parametric analysis. In this paper, the damage behaviour and the energy-absorbing results of composite sinusoidal specimens have been studied by quasi-static crushing experiments. The failure mechanisms of specimens under quasi-static crushing is further analysed. A numerical simulation has been performed by using the finite element model code LS-DYNA. The numerical results, in terms of load -displacement data, have been compared against experimental data, and good agreement has been found. Moreover, a sensitivity study has been carried out by varying material properties in order to assess their influence on the numerical results, and the material parameter selection scheme is optimised based on the constructed corresponding response surfaces. The results show that the response surface model has passed the test of goodness of fit, and the optimisation method can effectively assist the finite element modelling, and greatly decrease the numbers of trial and error.

Keywords: Composite sinusoidal specimen; energy-absorbing characteristics; failure mode; finite element model; optimisation method

1.0 INTRODUCTION

Crashworthiness design, verification and certification of transport category aircraft are significantly important for civil aviation safety, and the survivability of passengers and crews can be further enhanced by improving the crashworthiness design of aircraft structures, such as aircraft fuselage structures, cabin internal layouts and facilities[1–3]. In recent years, composite materials have been used more and more in aircraft structures and gradually applied to the main load-bearing structures. The crashworthiness design and verification of composite aircraft structures mainly rely on the engineering experiences for a long period of time. But the behaviour of composite materials under crash conditions poses particular challenges for engineering analysis. Because it requires modelling beyond the elastic region and into failure initiation and propagation[4].

The commercial finite element software codes are developed because of these disadvantages for engineering experiments, such as long design cycles, high costs, poor repeatability, etc. These commercial mainstream codes, such as LS-DYNA, ABAQUS, MSC.Dytran and PAM-CRASH, are available to use for crash simulations of composite aircraft structures[5–8], and offer built-in material models for composite structures, and each material model utilises different modelling strategy, which includes failure criterion, degradation scheme, material properties, and usually a set of model-specific input parameters that are typically needed for the computation, but do not have an immediate physical meaning[4]. So, the combination methods of extensive simulations and little experiments, and the establishment and development of simulation analysis method on crashworthiness of composite structures have become important research works.

The crashworthiness studies of composite aircraft structures had been conducted earlier by the United States NASA (National Aeronautics and Space Administration) Langley Research Center. In the late 1990s, many full-scale crash tests of composite aircrafts, such as Beech Starship, CirrusSR-20 and Lancair etc, had been conducted, and the test results showed that these composite aircrafts had perfect crashworthiness capabilities[9,10], and then the in-depth researches were conducted for composite aircraft structures. FAA (Federal Aviation Administration) also conducted many full-scale drop tests and crashworthiness researches of composite aircraft structures involving fibre reinforced materials and issued Advisory Circular AC 20–107B "composite aircraft structure" on September 8, 2009, to provide the airworthiness certification guidance information and acceptable compliance means. The Special Condition 25-362-SC had been issued for the crashworthiness of B787 on September 26, 2007, and B787 must meet the following four crashworthiness criteria for a range of aircraft vertical descent velocities up to 30 ft/sec, such as retention of items of mass, maintenance of acceptable acceleration and loads experienced by the occupants, maintenance of a survivable volume, and maintenance of occupant emergency egress paths.

The European Union had also conducted many crashworthiness research projects, such as the project "CRASHWORTHINESS" and "CRASURV" (The Design for Crash Survivability). The ONERA-Lille and AIRBUS France had redesigned the A320 fuselage frames, and the energy-absorbing sinewave beams were located in the under-floor part of fuselage section. The Netherlands NLR (National Aerospace Laboratory) manufactured the composite sinusoidal specimen and conducted the static tests. The German DLR (Deutsches Zentrum für Luft-und Raumfahrt) was responsible for the dynamic crushing tests. The French CEAT (Centre d'Essais Aéronautiques de Toulous) carried out the crashworthiness tests of fuselage section with subfloor composite sinusoidal specimens and eventually put forward a complete set of crashworthy test methods for composite aircraft based on the crashworthiness researches[11,12]. EASA (European Aviation Safety Agency) also issued

Acceptable Means of Compliance AMC 20–29 "composite aircraft structure" on July 26, 2010, but the technical content of this AMC was harmonised with FAA Advisory Circular AC 20–107B.

At the same time, the research scholars had done a lot of researches of composite aircraft structures with the combination methods of test and simulation with varying degrees of success, for circular tubes[13,14], square tubes[15-17], C channels[18], corrugated composite plates[4] and fuselage section[3,6,19-24]. Carruthers et al suggested that the closed-section tubes had evident effects on the crush performance. In particular, the stacking sequence can significantly affect the crush behaviour because the hoop fibres constrain the axial fibres and prevent them from splaying, thereby suppressing the propagation of the crush front[35]. Riccio et al. proposed a user-defined 3D damage model (VUMAT) with solid elements implemented into the finite element code Abaqus/Explicit, and they also supplied a numerical analysis on an omega-stiffened laminate panel under low-velocity impacts[32,33]. Pietropaoli and Riccio benefited from an existing procedure based on the combined use of the Virtual Crack Closure Technique and the fail release approach for the analysis of delamination growth phenomena in composite structures[34].

The aerospace community has focused mostly on test specimens that resemble subfloor structures, such as floor beams, stanchions, and stiffeners. The test element geometries are open section, such as semicircular segments[40], C-channels[18,41], and the DLR omega specimen[42]. Feraboli et al. conducted the experiments, simulation and optimisation design studies of cargo sub-floor composite C channels based on the "building block" approach of FAA AC 20–107B, the failure process and failure modes of composite C channels can be more accurately simulated by the developed finite element models, the tests and simulation of details, sub-components and components would be further carried out in order to study the crashworthy performance of composite fuselage section in detail[25]. Corrugated web geometries have a history of being employed as energy absorbers in the subfloors of aircraft to improve crashworthiness in both rotorcraft[36,37] and large commercial transport aircraft[38]. Corrugation increases the stability of vertical web, thereby increasing its crippling strength, and enables floor beams to carry higher design loads. The corrugated geometry promotes stable crushing and significant energy absorption during the crash events by reducing the likelihood of macroscopic buckling[39]. Ren et al. conducted numerical investigations to evaluate the influence of stacking sequence, progressive damage model, trigger geometry on energy absorption characteristics of fabric and unidirectional composite sinusoidal plates[44,45]. With the increasing use of composite material structures in aircraft fuselage section, there is a need to further conduct the crashworthiness tests and simulation of composite aircraft structures.

This paper aims to build the progress-crushing finite-element model of the composite sinusoidal corrugated and analysis the model with parameters. This paper mainly focuses on the crashworthiness indicator-specific energy absorption. Section 3 mainly details the quasi-static crushing test of the composite sinusoidal corrugated. The single-layer finite element model of composite sinusoidal specimen was developed in HyperMesh, and the correctness of MAT 54 composite material model and finite element model of composite sinusoidal specimens were verified based on the nonlinear finite element code LS-DYNA. In the section 4, finite element model of the composite sinusoidal corrugated is build. The last two sections carry out the parametric analyses. At first, the sensitivity analysis of MAT 54 material model parameters is conducted, and the nonlinear mapping relationships between the Special Energy Absorption and material model parameters are obtained by using the orthogonal design methods. At last, the material parameter selection scheme was optimised based on the constructed corresponding response surfaces.
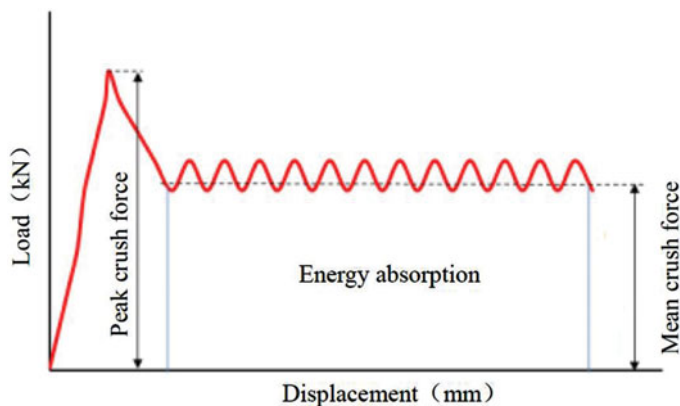
Figure 1. (Colour online) Typical load-displacement curve.

2.0 CRASHWORTHINESS EVALUATION INDICATORS

For thin-walled energy-absorbing structures, the typical load-displacement curve during the crushing process is shown in Fig. 1. The crashworthiness evaluation indicators are defined to evaluate the crashworthiness of energy-absorbing structures, such as energy absorption (E_A), specific energy absorption (*SEA*), peak crush force (F_{max}), and mean crush force (F_{mean})[43].

Specific Energy Absorption (*SEA*): The absorbed energy (E_A) per unit mass (m) of crushed structure. The ability of material to dissipate energy can be expressed in terms of *SEA*, which has units of J/g, and the higher value indicates the greater energy absorption efficiency of a material. The equation for *SEA* is:

$$SEA = \frac{E_A}{m} = \frac{\int F dl}{m} = \frac{\int F dl}{\rho \cdot A \cdot l},\qquad\qquad \dots (1)$$

where F is the crushing force with the function of the displacement l, ρ is the density, and A is the cross-sectional area.

Peak Crushing Force (F_{max}) is the threshold value of structural crushing damage to evaluate the difficulty level of the energy absorption of the structure under forcing, which is the initial peak value of the load-displacement curve.

Mean Crushing Force (F_{mean}) is the average force of the whole crushing process, as given by Equation (2):

$$F_{mean} = \frac{\int F ds}{S},\qquad\qquad \dots (2)$$

where F is the crushing force, s is the vertical crushing displacement, and S is the total crushing displacement of the whole crushing process.

(a) Sectional geometry
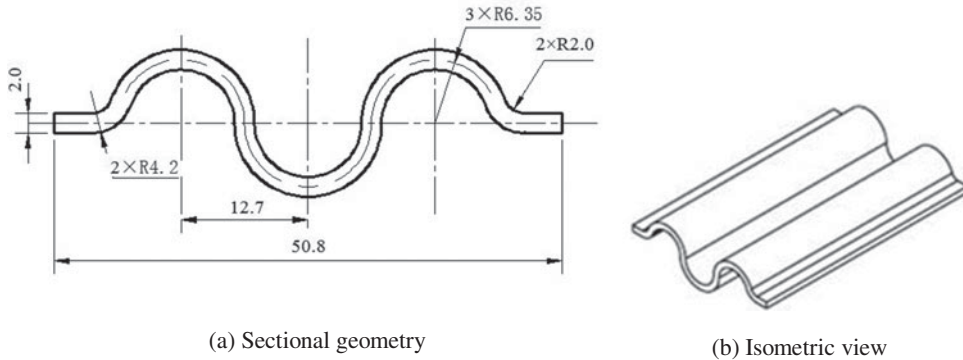
(b) Isometric view

Figure 2. Composite sinusoidal specimen geometries and dimensions (all dimensions in mm).

3.0 QUASI-STATIC CRUSHING TEST

The detailed dimensions of composite sinusoidal specimen are shown in Fig. 2(a), the length of composite sinusoidal specimen is 76.2 mm, the width is 50.80 mm, and the thickness is 2 mm. The isometric view of composite sinusoidal specimen is shown in Fig. 2(b).

The preparation and tests of composite coupons and composite sinusoidal specimens were conducted in AVIC Beijing Institute of Aeronautical Materials at Beijing, China. The composite sinusoidal specimens are manufactured by press-molding through the steel matching tool, shown in Fig. 3(a). The material system is T700/3234, it is a unidirectional tape 12k tow, and a 270 $°F$ (132 °C) cure resin designated for autoclave or oven-only cure. The preparation of composite corrugated plate has experienced the process of paving, curing and mold releasing. The composite sinusoidal specimen is shown in Fig. 3(b). In order to initiate the steady crushing progress, the 45-degree chamfer sided weakness is set up at the top of composite sinusoidal specimen. The composite sinusoidal specimen consists of 16 layers of unidirectional laminates with orientations $(0°/90°)_{4s}$, and each layer thickness is 0.125 mm.

The uniform crushing rate is 2.5 mm/min, and the typical morphology of composite sinusoidal specimen after crush testing is shown in Fig. 4(a). The interlaminar cracks formed and grew at the interface of adjacent layers, and the intralaminar cracks form and grow within individual layers. We can see the intralaminar cracks, 0° layers and 90° layers, the lamina bundles exhibit significant bending deformation, but do not fracture. The failure mode of composite sinusoidal specimen is lamina bending failure mode, and the lamina bending failure mode is characterised by very long interlaminar cracks, intralaminar cracks, and lamina bundles, as shown in Fig. 4(b) and Fig. 4(c)[26].

The synchronous data acquisition system of Instron electronic universal testing machine records the crushing load and displacement data during the crushing process. The quasi-static crushing load-displacement curve is shown in Fig. 5. The OA stage is an approximately linear variation before collapse, and the load is increased to the initial peak crush force (Point A). The collapse then occurs at the top of specimen, and results in a reduction of crushing load (AB stage). The progressive crushing process occurs and the crushing load remained at a relatively stable level (BC stage). The total energy absorption is represented by the area below the curve OABC. The calculating SEA value is 72.47 J/g for the composite sinusoidal specimen based on the Equation (1)[24].
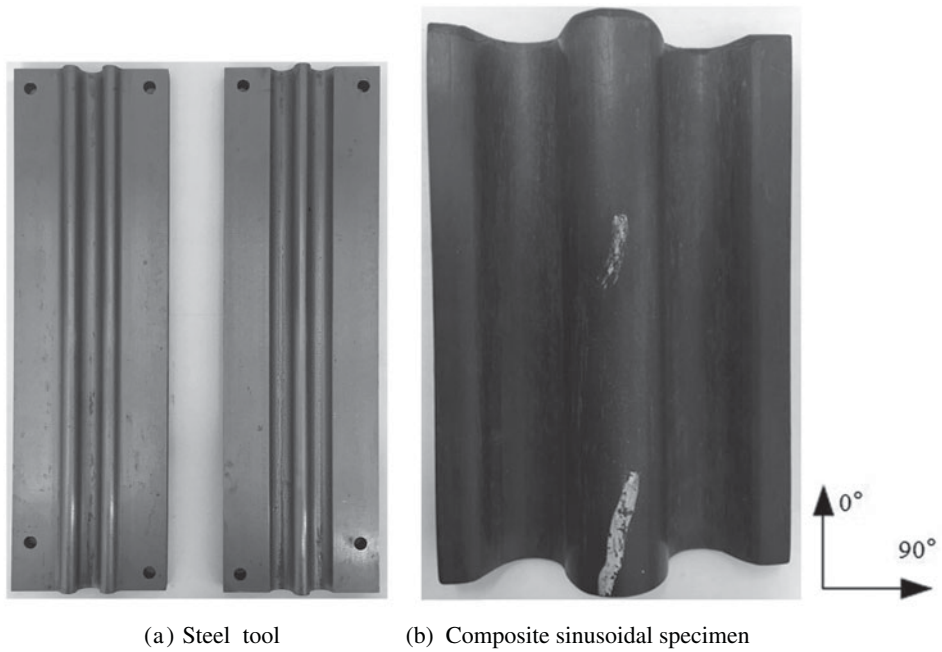
(a) Steel tool   (b) Composite sinusoidal specimen

Figure 3. Steel tool and composite sinusoidal specimen.

(a) Crushing test failure modes

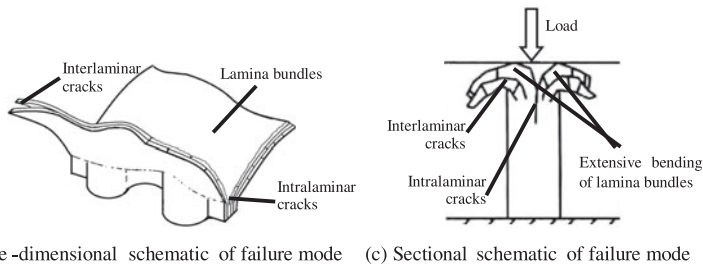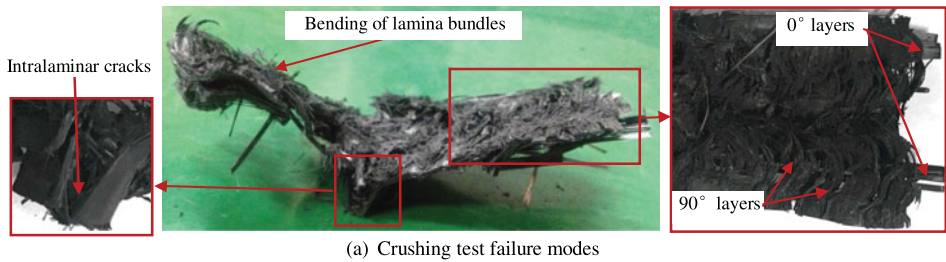(b) Three-dimensional schematic of failure mode   (c) Sectional schematic of failure mode

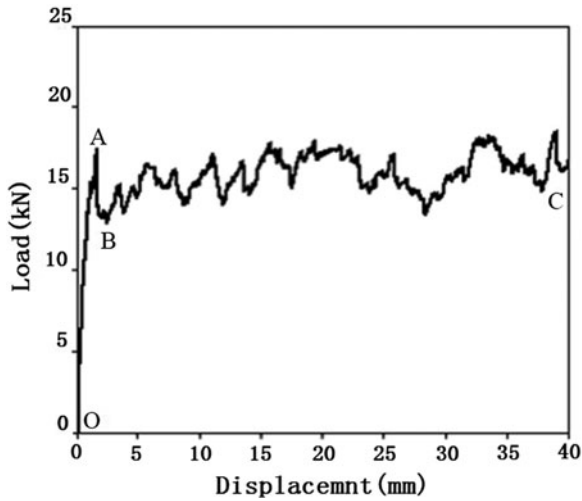Figure 4. (Colour online) Crushing characteristics of lamina bending crushing mode
of composite sinusoidal specimen.

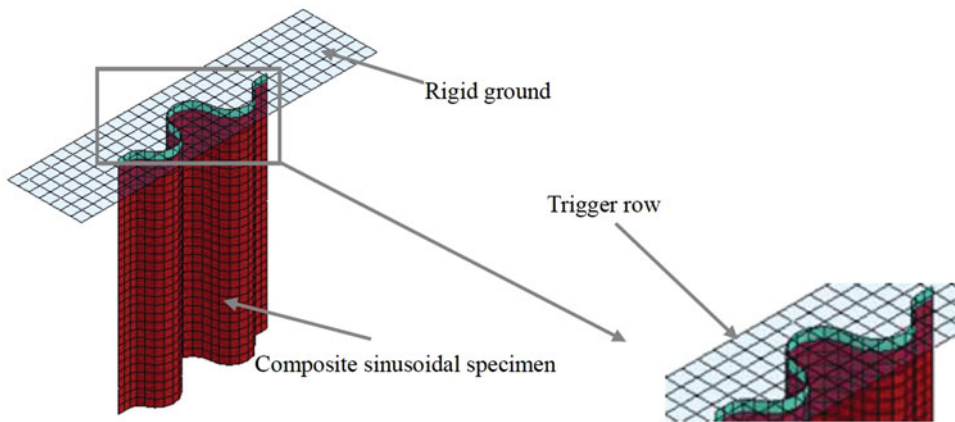Figure 5. Quasi-static crushing load-displacement curve.

Figure 6. (Colour online) Finite element model of composite sinusoidal specimen and trigger row.

4.0 FINITE ELEMENT MODEL AND MATERIAL MODEL

4.1 Finite element model

As shown in Fig. 6, the LS-DYNA model includes the composite sinusoidal specimen, the trigger row, and the rigid ground. The shell element is commonly used in crashworthiness simulation of aircraft fuselage section, and the fully integrated shell element (formulation 16) is adopted for the finite element model of composite sinusoidal specimen, because it can calculate internal energy absorption accurately, simulate bucking accurately, and calculate very fast[4,24,27]. Based on the mesh sensitivity analysis of shell elements, the finite element model of composite sinusoidal specimen is modelled with a total of 840 shell elements of 2.54 mm × 2.54 mm[46], having constant thickness of 2 mm. The 45-degree chamfer is modelled as a single row of reduced-thickness 0.25-mm elements at the crush front of the specimen.

Table 1
Material properties of T700/3234

Symbol	Title	Value
ρ	Density	1.53 g/cm^3
E_a	Young's modulus in longitudinal (fibre) direction	128 GPa
E_b	Young's modulus in transverse (perpendicular to fibre) direction	8.4 GPa
G_{ab}	Shear modulus in ab plane	4.0 GPa
G_{bc}	Shear modulus in bc plane	4.0 GPa
G_{ca}	Shear modulus in ac plane	4.0 GPa
P_{rab}	Minor Poisson's ratio	0.0218
X_t	Longitudinal tensile strength (fibre direction)	2093 MPa
X_c	Longitudinal compressive strength (fibre direction)	1060 MPa
Y_t	Transverse tensile strength (perpendicular to fibre)	50 MPa
Y_c	Transverse compressive strength (perpendicular to fibre)	198 MPa
S_c	Shear strength in ab plane	104 MPa

Table 2
Strain-limits and failure parameters of MAT 54

Symbol	Title	Value
DFAILT	Max strain for fibre tension	0.0174
DFAILC	Max strain for fibre compression	−0.02
DFAILM	Max strain for matrix straining in tension and compression	0.024
DFAILS	Max shear strain	0.03
BETA	Weighing factor for shear term in tensile fibre mode	0.5
FBRT	Softening factor for fibre tensile strength after matrix failure	0.5
YCFAC	Softening factor for fibre compressive strength after matrix failure	1.2
TFAIL	Time step size criteria for element deletion	1.153e^{-9}
SOFT	Crush front strength reducing parameter	0.70
EFS	Effective failure strain	0

The card * PART_COMPOSITE is used to define the 16 layers of composite sinusoidal specimen, and the finite element model is adopted the material model of MAT 54_Enhanced_Composite_Damage, which used the Chang-Chang failure criterion in the LS-DYNA theoretical manual[27,28]. The material stress-strain curves in the elastic region follows the linear elastic theory. The composite materials can successfully be modelled by MAT54 which has been approved based on the single-element simulations[29]. The material card of MAT 54 contains input parameters for both material physical properties of T700/3234 (Table 1) and other code-specific parameters (Table 2)[4,27]. The material model of MAT 20_Rigid is selected for rigid ground, and the input parameters of material card of MAT 20 are shown in Table 3[24,27].

Table 3
Material parameters of rigid ground

Symbol	Title	Value
ρ	Density	7.9 g/cm^3
E	Modulus of elasticity	210 GPa
μ	Poisson's ratio	0.3

4.2. Boundary conditions and contact definitions

For the finite element model of composite sinusoidal specimen, a fixed boundary condition was assigned to the bottom nodes along the flat end of all finite element models, and the top nodes were completely free. All degrees of freedom of the rigid wall are constrained except plane normal, so that it can only move along the height of the corrugated plate. In order to reduce the computation time, speed scaling is carried out in this example, the constant pressure velocity of the rigid wall is applied to 3800mm/s, and the total displacement is about 40 mm. Because the strain rate effect is not considered in the material-model parameter setting, and the speed scaling has little effect on the simulation results after several tests, the setting of the loading speed is reasonable[24].

The contact definition between the rigid ground and the composite sinusoidal specimen is necessary for the two parts to properly interact, and the Rigid_Nodes_to_Rigid_Body Contact algorithm is just selected, the static friction factor and dynamic friction factor are 0.3, respectively. For the contact algorithm. This is accomplished by allowing the nodes of the composite sinusoidal specimen to penetrate into the platen by a specified distance. As the nodes penetrate, they are resisted by the forces calculated based on a user-specified load-penetration curve. In this contact definition, the initial load-penetration curve defines the reaction normal force, such a –load-penetration curve is necessary in the contact definition when using the MAT 54 material model. Varying the –load-penetration curve has an important effect on the stability of the model, yet there is no way of knowing *a priori* of deterring experimentally the correct shape. The initial load-penetration curve was estimated from the compressive failure load and cross-sectional area of the element. It was subsequently fine-tuned to ensure that at least two rows of elements penetrated the platen prior to any element deletion[30,46]. Figure 7 shows the selected load-penetration curve.

5.0 FINITE ELEMENT MODEL SIMULATION

The simulation failure modes of composite sinusoidal specimen, as shown in Fig. 8, reveal that failure advances in an even and stable mode, through elements deletion at the crush front. When the first ply in an element fails, the elements remain in the straight position and do not exhibit a different morphology. Once all plies fail, the elements are immediately deleted. Once an element is deleted, the entire row of elements is also deleted. Therefore, the crush progresses with a progressive deletion of the crush front row of elements are achieved without any other graphic indication.

The simulation load-displacement curves are shown in Fig. 9 in its raw and filtered state. The raw curve is characterised by an alternating series of sharp peaks and valleys, giving it a saw tooth appearance. A low-pass digital filter was used to filter numeric results. When the
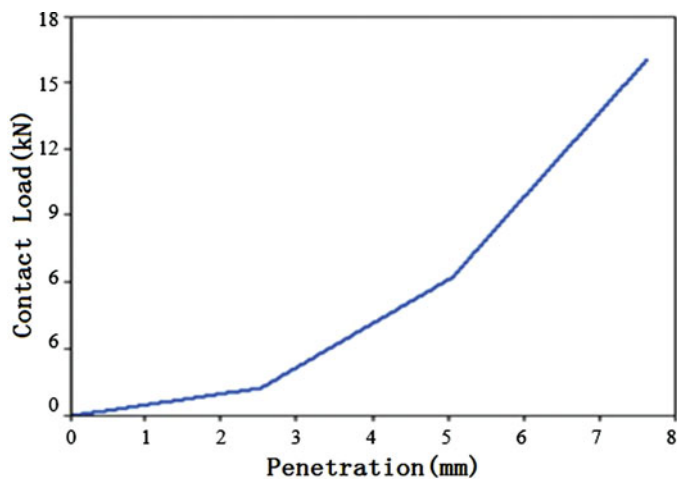
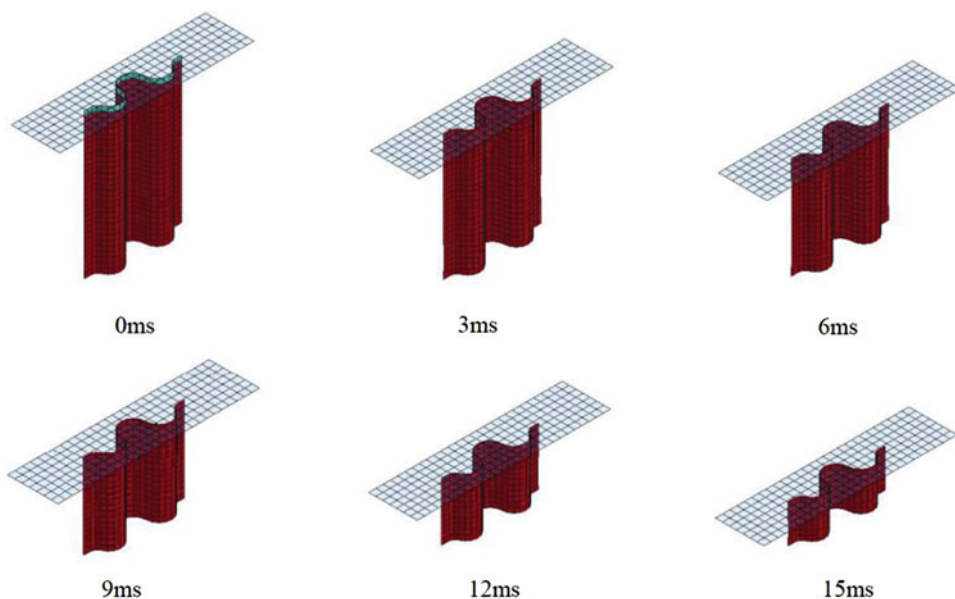Figure 7. (Colour online) –Load-penetration displacement curves used in contact definition.

Figure 8. (Colour online) Time progression of the baseline simulation showing
stable element row deletion.

simulation curve is filtered by SAE 600 Hz, the mean crush force remains unchanged, but the peaks and valleys are smoothed. The curve oscillates about the mean crush force without large variations in local peak values, indicating that the simulation is stable. While the simulation curve is filtered by SAE 300 Hz, the mean crush force also remains unchanged, but there are no peaks and valleys. All of the simulation curves are filtered by SAE 600 Hz[16,17,31].

The filtered simulation load-displacement curve is compared with the experimental curve in Fig. 10. The simulation captures the key characteristics of experimental curve: peak crush force, mean crush force, and *SEA* value. The simulated mean crush force F_{mean} value is
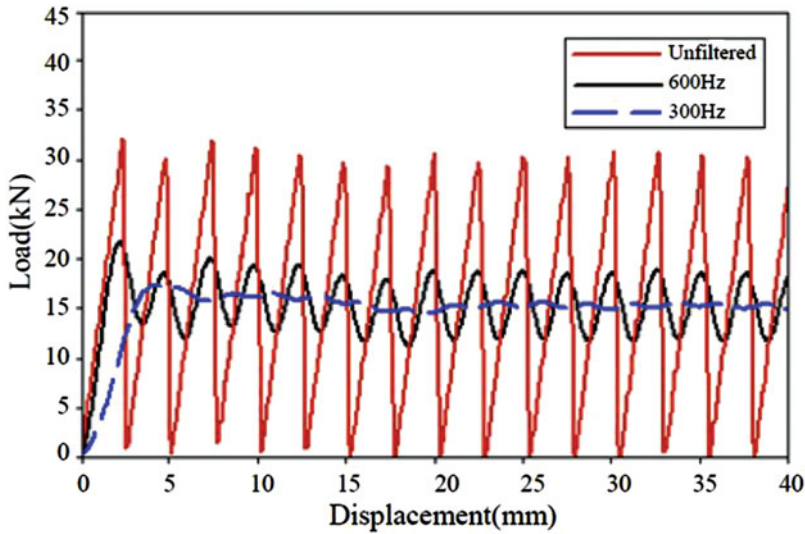
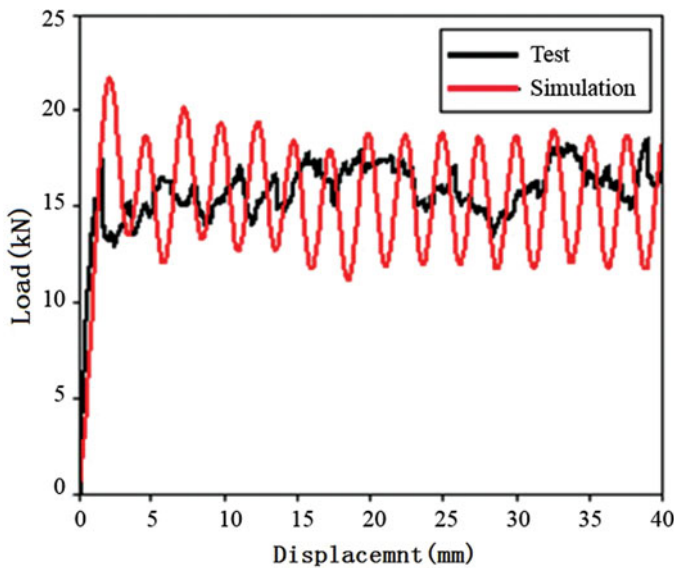Figure 9. (Colour online) Load-displacement curve under different SAE filter frequency.

Figure 10. (Colour online) Experimental and model baseline load-displacement curves.

17.15 kN, compared to the experimental 18.11 kN, the difference is –5.3%; The simulated *SEA* value is 69.98 J/g, compared to the experimental 72.47 J/g, the difference is –3.44% which is within a little and acceptable range. The material model MAT 54 of composite sinusoidal specimen can captures all the experimental significant features, and the simulation *SEA* value is highly agreed with the experimental value, which can validate the correctness of finite element model, so the material model MAT 54 can also be used to successfully simulate the behaviour of composite sinusoidal specimens undergoing axial crushing.
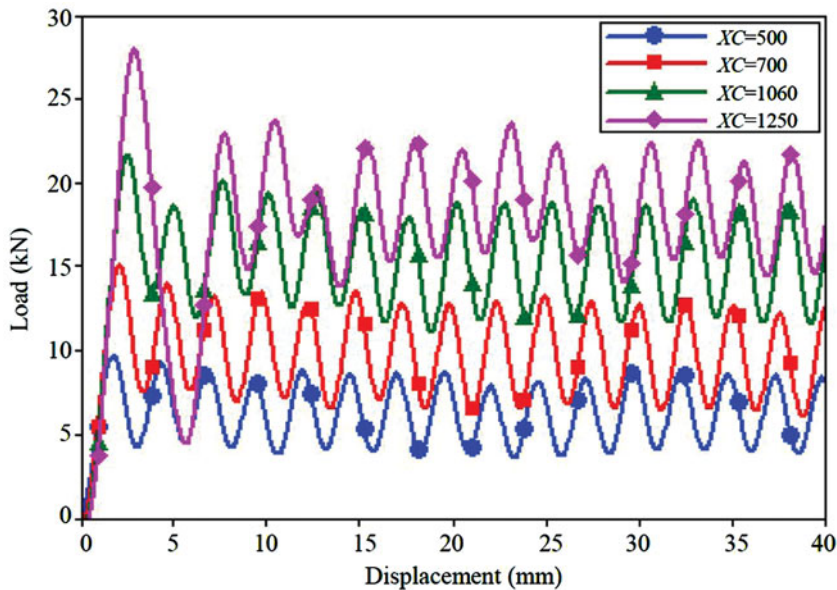
Figure 11. (Colour online) Simulation load-displacement curves with different *XC* values.

6.0 SENSITIVITY ANALYSIS OF MATERIAL MODEL PARAMETERS

An effective model needs to be sufficiently robust to tolerate small variations in material property input data of MAT 54 material model, to accommodate small errors in measured strength and stiffness. Yet, some non-physical model calculation parameters set of MAT 54 material model will have a greater impact on the results[4,30]. However, LS-DYNA User's Manual is not described in detail for influence mechanism of parameters on simulation results during progressively crushing failure[27]. The sensitivity of the model to variations in MAT 54 material model parameters, i.e. *XC*, *DFAILC*, *SOFT*, should be discussed. The control variable method was used to study the effects of *XC*, *DFAILC*, and *SOFT* parameters on the simulation results based on the above verified finite element model of composite sinusoidal specimens.

The *XC* is the material properties, and can be measured by the material performance test, but there is a large dispersion for the test *XC* results. The sensitivity analysis of this parameter has become very important for the simulation results. The load-displacement curves with different *XC* values were show in Fig. 11, the varying *XC* has a great effect on the resulting load-displacement curve. Small decreases in *XC* values (500 MPa, 700 MPa) significantly lower the mean crush force, while small increments of *XC* value (1250 MPa) significantly raise the mean crush force, at least until a stability threshold is reached and the model becomes unstable, with the irregular element elimination of failure mode. This is true within an envelope of stable values, beyond which the model became unstable.

The simulation load-displacement curve under different *DFAILC* values were shown in Fig. 12, the changing of *DFAILC* can change the average crushing load. Reducing *DFAILC* (making it more negative) increases the mean crush force, while increasing *DFAILC* (making it less negative) decreases the average load value. Based on these results, the compressive strain-to-failure in the fibre direction, *DFAILC*, has a more profound effect on the results of
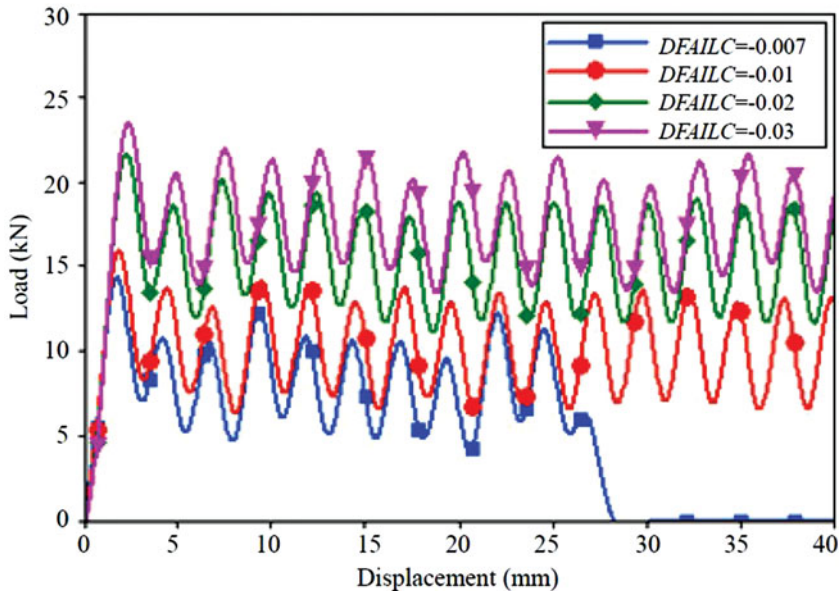
Figure 12. (Colour online) Simulation load-displacement curves with different *DFAILC* values.

the simulation, and it is a primary failure mode for the given specimen geometry-material combination, and therefore a critical parameter for achieving successful simulation results.

The *SOFT* is a non-physical parameter, which is different from the material performance parameter and cannot be measured experimentally or by theoretical calculation. It can be used to reduce the strength of the front of a row of crushing element in order to avoid the global buckling failure. The sensitivity of the model to variations in the *SOFT* parameter is investigated within the admissible range (0, 1), as shown in Fig. 13. It is capable of dictating whether the simulation is stable or unstable, and increasing the *SOFT* value has the effect of increasing the mean crush force and *SEA* of the simulation. Increasing the *SOFT* value has the effect of increasing the mean crush force and *SEA* of the simulation. Lowering the *SOFT* parameter has the effect of lowering the mean crush force and *SEA* value of the simulation. Determining the correct value of the *SOFT* parameter is a challenging task, but it can be found by trial and error until the load-displacement curve of the simulation matches the experimental result. Unless the right *SOFT* value is found and utilised, it is impossible to obtain a successful simulation.

7.0 ORTHOGONAL EXPERIMENTS OPTIMISATION ANALYSIS

Based on the above analysis, there are three parameters i.e., *XC*, *DFAILC*, *SOFT*, which have significant effects on energy-absorbing results of composite sinusoidal specimens, and presents a certain regularity. In order to study the influence of the three parameters on simulation results in depth and decrease the number of trials and errors, the response surface method (RSM) was adopted to construct the mapping relationships among the *SEA*, *XC*,
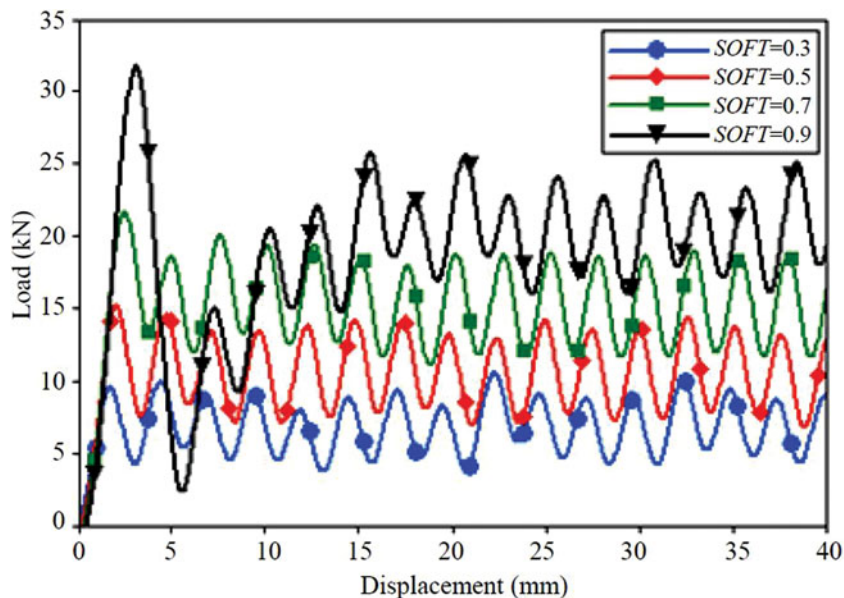
Figure 13. (Colour online) Simulation load displacement curves with different *SOFT* values.

DFAILC and *SOFT* and the simulation results were closed to the experimental values through the quadratic polynomial fitting and objective optimisation.

The 'Trial-Assessment-Correction' method is used to determine an approximate interval value of three parameters i.e., the design scope of variables, under the condition of simulation model stability calculation:

$$1000\text{MPa} \leq XC \leq 1100\text{MPa}$$
$$0.65 \leq SOFT \leq 0.75 \qquad \text{The optimal object}: SEA \rightarrow 72.47$$
$$-0.0150 \leq DFAILC \leq -0.0300$$

The orthogonal test is designed based on the numbers of design variables and the design scopes, and the 15 sets of calculation are carried out in the whole orthogonal experiment, which set up 3 centre repeat points. Through the simulation calculations of composite sinusoidal specimens under quasi-static crushing, the corresponding *SEA* value and the relative difference compared with the test result are shown in Table 4.

Based on the orthogonal simulation results, the nonlinear mapping relationships between the *SEA* and *XC*, *SOFT* and *DFAILC* parameters are obtained by using the least square method. The quadratic response surface function is obtained by setting *XC* for X_1, *SOFT* for X_2, and *DFAILC* for X_3:

$$SEA = -263.35125 + 0.13713X_1 + 386.275X_2 - 2869X_3 - 0.09X_1X_2 - 1.00667X_1X_3$$
$$-1353.33333X_2X_3 - 9.0 \times 10^{-6}X_1^2 - 147X_2^2 - 77333.33333X_3^2$$

The fitting coefficients of the quadratic model are shown in Table 5, and the response surfaces among the *SEA*, *XC*, *SOFT* and *DFAILC*, are constructed, as shown in Fig. 14. The coefficient of variance analysis R^2 is 0.9995, but the adjusted coefficient of variance analysis

Table 4
The orthogonal simulation table of composite sinusoidal specimens

Parameter Number	XC (MPa)	SOFT	DFAILC	SEA (J/g)	Difference (%)
1	1050	0.75	−0.0150	63.22	−12.76
2	1050	0.70	−0.0225	73.42	+1.31
3	1050	0.65	−0.0150	53.07	−26.77
4	1100	0.75	−0.0225	82.88	+14.36
5	1050	0.70	−0.0225	73.42	+1.31
6	1000	0.70	−0.0150	55.31	−23.68
7	1100	0.70	−0.0150	62.10	−14.31
8	1000	0.70	−0.0300	75.24	+3.82
9	1050	0.75	−0.0300	85.35	+17.77
10	1050	0.65	−0.0300	73.17	+0.97
11	1100	0.65	−0.0225	71.21	−1.74
12	1100	0.70	−0.0300	83.54	+15.28
13	1000	0.75	−0.0225	75.30	+3.91
14	1000	0.65	−0.0225	62.73	−13.44
15	1050	0.70	−0.0225	73.42	+1.31

Table 5
Fitting coefficient of quadratic model

Item	Coefficient
X_1	0.13713
X_2	386.275
X_3	−2869
X_1^2	-9.0×10^{-6}
X_2^2	−147
X_3^2	−77333.33333
X_1X_2	−0.09
X_1X_3	−1.00667
X_2X_3	−1353.33333
constant	−263.35125

R^2_{adj} is 0.9986, which shows that the goodness of fit is higher. The residual of the fitting is 0.6665.

According to the optimisation objectives, the setting of parameters is optimised based on the response surface data. Considering that XC is a material performance parameter, and $XC = 1060$ MPa is used as the final optimisation results. The final optimisation results and the simulation results based on the optimal design variables are presented in Table 6. The calculated SEA value is 72.4699 J/g based on the response surface model, which is very close to the experimental SEA value of 72.47 J/g, and compared to the simulated SEA value 73.6418 J/g, the difference is only 1.62%, which indicates the accuracy of the parameters optimisation based on the response surface model, and also shows that it is feasibility to help to select the simulation parameters by using the response surface method.
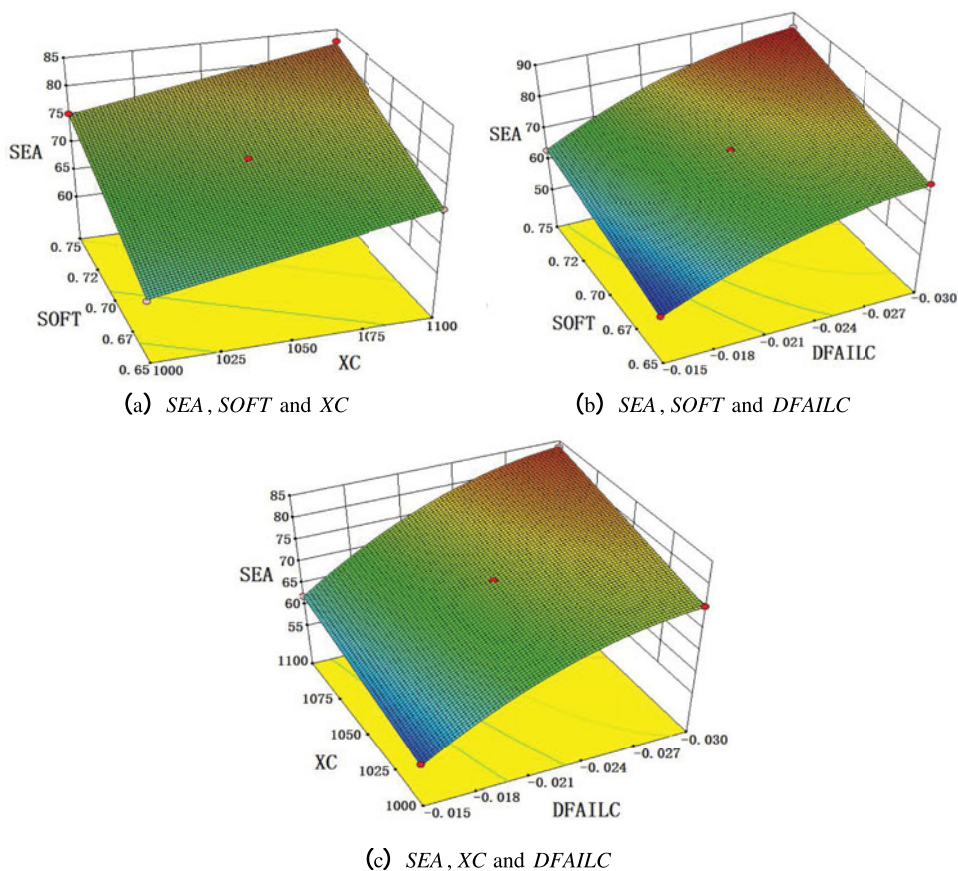
(a) *SEA*, *SOFT* and *XC*

(b) *SEA*, *SOFT* and *DFAILC*

(c) *SEA*, *XC* and *DFAILC*

Figure 14. (Colour online) Quadratic response surfaces of *SEA* and different
material model parameters (*XC*, *SOFT*, *DFAILC*)

Table 6
Comparison of parameters optimisation design and simulation

Result	XC (Mpa)	SOFT	DFAILC	SEA (J·g^{-1})
RSM	1060	0.73	−0.0197	72.4699
Simulation	1060	0.73	−0.0197	73.6418
Difference	-	-	-	1.62%

8.0 CONCLUSION

Based on the failure mode and test results of composite sinusoidal specimens under quasi-static crushing, the finite element model of composite sinusoidal specimen is developed, which can accurately simulate the load-displacement curve and the SEA value, but the finite element model cannot provide insight into the failure morphology.

The paper aims to build the progress-crushing finite element model of the composite sinusoidal corrugated and carry out the parametric analysis. A numerical simulation has been performed by using the finite element model code LS-DYNA. Through a sensitivity study

of different parameters of MAT 54 material model, it is shown that *XC* and *DFAILC* are the primary material parameters leading to element failure and deletion. *SOFT* is the single most influential parameter, and can be calibrated by trial-and-error to achieve the success of the simulation. The nonlinear mapping relationships between the *SEA* and parameters (*XC*, *DFAILC*, *SOFT*) was obtained based on the orthogonal design and response surface method. The results showed that the response surface model has a higher the goodness of fit, and the optimisation method can effectively assist the finite element modelling, and greatly the numbers of trial and error.

UNCITED REFERENCES:

ACKNOWLEDGEMENTS

REFERENCES

1. DAMODAR, R.A. and MARSHALL, R. Design and evaluation of composite fuselage panels subjected to combined loading conditions, *J Aircr*, 2005, **42**, (4), pp 1037-1045. doi: 10.2514/1.18994.

2. FASANELLA, E.L. and JACKSON, K.E. Crash simulation of a vertical drop test of a B737 fuselage section with auxiliary fuel tank, U.S. Army Research Laboratory, Vehicle Technology Center, Langley Research Center, April 2000. https://www.fire.tc.faa.gov/2001Conference/files/CrashAnalyticalModelingSimulation/EFasanellaPAPER.pdf

3. ZOU, T.C., MOU, H.L. and FENG, Z.Y. Research on effects of oblique struts on crashworthiness of composite fuselage sections, *J Aircr*, 2012, **49**, (6), pp 2059-2063. doi: 10.2514/1.C031867.

4. FERABOLI, P., WADE, B., DELEO, F., RASSAIAN, M., HIGGINS, M. and BYAR, A. LS-DYNA MAT54 modeling of the axial crushing of a composite tape sinusoidal specimen, *Composites: Part A*, 2011, **42**, (11), pp 1809-1825. doi: 10.1016/j.compositesa.2011.08.004.

5. DAMODAR, R.A. and MARSHALL, R. Design and evaluation of composite fuselage panels subjected to combined loading conditions, *J Aircr*, 2005, **42**, (4), pp 1037-1045. doi: 10.2514/1.18994.

6. FENG, Z.Y., MOU, H.L., ZOU, T.C. and REN, J. Research on effects of composite skin on crashworthiness of composite fuselage section, *Int J Crashworthiness*, 2013, **18**, (5), pp 459-464. doi: 10.1080/13588265.2013.805291.

7. HEIMBS, S., HOFFMANN, M., WAIMER, M., SCHMEER, S. and BLAUROCK, J. Dynamic testing and modelling of composite fuselage frames and fasteners for aircraft crash simulations, *Int J Crashworthiness*, 2013, **18**, (4), pp 406-422. doi: 10.1080/13588265.2013.801294.

8. WIGGENRAAD, J.F.M., MICHIELSEN, A.L.P.J., SANTORO, D., LEPAGE, F., KINDERVATER, C. and BELTRAN, F. Development of a crashworthy composite fuselage structure for a commuter aircraft, NLR-TP-99532, National Aerospace Laboratory NLR, 1999, pp 1-23.

9. TERRY, J.E. Design and test of an improved crashworthiness small composite airplane, SAE Paper 2000-01-1673, Presented at the SAE General Aviation Technology Conference and Exposition, Wichita, KS, 2000, pp 1-18. doi: 10.4271/2000-01-1673.

10. TERRY, J.E., HOOPER, S.J. and NICHOLSON, M. Design and test of an improved crashworthiness small composite airplane, NASA/CR-2002-211774, NASA, Washington, DC, 2002, pp 1-228. https://ntrs.nasa.gov/search.jsp?R=20020068132.

11. DAVID, D., DIDIER, J., MICHEL, M. and GÉRARD, W. Evaluation of finite element modeling methodologies for the design of crashworthy composite commercial aircraft fuselage, 24th International Congress of the Aeronautical Sciences, 2004, pp 1-10. http://www.icas.org/ICAS_ARCHIVE/ICAS2004/PAPERS/071.PDF.

12. Wiggenraad, J.F.M., Santoro, D., Lepage, F., Kindervater, C. and Mañez, H.C. Development of a crashworthy composite fuselage concept for a commuter aircraft, NLR-TP-2001-108, National Aerospace Laboratory NLR, 2001, pp 1-13.

13. Huang, J.C. and Wang, X.W. Numerical and experimental investigations on the axial crushing response of composite tubes, *Composite Structures*, 2009, **91**, (2), pp 222-228. doi: 10.1016/j.compstruct.2009.05.006.

14. Mamalis, A.G., Manolakos, D.E., Ioannidis, M.B. and Papapostolou, D.P. The static and dynamic axial collapse of CFRP square composite tubes: Finite element modeling, *J Composite Structures*, 2006, **74**, (2), pp 213-225. doi: 10.1016/j.compstruct.2005.04.006.

15. Palanivelu, S., Paepegem, W., Degrieck, J., Kakogiannis, D., Ackeren, J. and Hemelrijck, D. Parametric study of crushing parameters and failure patterns of pultruded composite tubes using cohesive elements and seam, Part I: Central delamination and triggering modeling, *Polymer Testing*, 2010, **29**, (6), pp 729-741. doi: 10.1016/j.polymertesting.2010.05.010.

16. Xiao, X.R. Modeling energy absorption with a damage mechanics based composite material model, *J Composite Materials*, 2009, **43**, (5), pp 427-444. doi: 10.1177/0021998308097686.

17. Xiao, X.R., Botkin, M.E. and Johnson, N.L. Axial crush simulations of braided carbon tubes using MAT58 in LS-DYNA, *Thin-Walled Structures*, 2009, **47**, (6-7), pp 2247-2259. doi: 10.1016/j.tws.2008.12.004.

18. Deleo, F., Wade, B., Feraboli, P. and Rassaian, M. Crashworthiness of composite structures: Experiment and simulation, Proceedings of the 50th AIAA Structures, Structural Dynamics and Materials Conference, 4–7 May 2009, Palm Springs, California, US.

19. Ilcewicz, L.B. and Brian, M. Safety & certification initiatives for composite airframe structure, 46th AIAA/ASME/ASCE/AHS/ASC structures, Structural Dynamics & Materials Conference, 18-21 April 2005, Austin, Texas, US.

20. Jackson, K.E. and Fasanella, E.L. Development of a scale model composite fuselage concept for improved crashworthiness, *J Aircr*, 2001, **38**, (1), pp 95-103. doi: 10.2514/2.2739.

21. Jackson, K.E. and Fasanella, E.L. Crash simulation of vertical drop tests of two Boeing 737 fuselage sections, DOT/FAA/AR-02/62, US Department of Transportation, Federal Aviation Administration, 2002, pp 1-96.

22. Jackson, K.E. and Fasanella, E.L. Development and validation of a finite element simulation of a vertical drop test of an ATR 42 regional transport airplane, DOT/FAA/AR-08/19, US Department of Transportation, Federal Aviation Administration, 2008, pp 1-81.

23. Waimer, M., Kohlgruber, D., Hachenberg, D. and Voggenreiter, H. Experimental study of CFRP components subjected to dynamic crash loads, *Composite Structures*, 2013, **105**, pp 288-299. doi: 10.1016/j.compstruct.2013.05.030.

24. Mou, H.L., Zou, T.C., Feng, Z.Y. and Xie, J. Crashworthiness analysis and evaluation of fuselage section with sub-floor composite sinusoidal specimens, *Latin American J Solids and Structures*, 2016, **13**, (6), pp 1187-1202. doi: 10.1590/1679-78252446.

25. Feraboli, P. Development of a corrugated test specimen for composite materials energy absorption, *J Composite Materials*, 2008, **42**, (3), pp 229-256. doi: 10.1177/0021998307086202.

26. Farley, G.L. and Jones, R.M. Crushing characteristics of continuous fiber-reinforced composite tubes, *J Composite Materials*, 1992, **26**, (1), pp 37-50. doi: 10.1177/002199839202600103.

27. Livermore Software Technology Corporation, LS-DYNA keyword user's manual, Version 971, 2006, Livermore, US.

28. Han, H.P., Taheri, F., Pegg, N. and Lu, Y. A numerical study on the axial crushing response of hybrid pultruded and ±45° braided tubes, *Composite Structures*, 2007, **80**, (2), pp 253-264. doi: 10.1016/j.compstruct.2006.05.012.

29. Bonnie, W., Paolo, F., Morgan, O. and Mostafa, R. Simulating laminated composite materials using LS-DYNA material model MAT54: Single-element investigation, DOT/FAA/TC-14/19, US Department of Transportation, Federal Aviation Administration, 2015, pp 1-63.

30. Deepak, S. Crashworthy design and analysis of aircraft structures, A Thesis Submitted to the Faculty of Drexel University. Doctor of Philosophy, 2013.

31. Johnson, A., David, M., CMH-17 Crashworthiness wg: round robin simulation of crash elements, In: Proc. 56th Polymer Matrix Composite Materials Handbook Meeting. Federal Aviation Authority (FAA), CMH-17 crashworthiness forum, 19-22 July 2010, Costa Mesa, California, US. http://elib.dlr.de/67372.

32. RICCIO, A., SAPUTO, S. and SELLITTO, A. A user defined material model for the simulation of impact induced damage in composite, *Key Engineering Materials*, 2016, **713**, pp 14-17. doi: 10.4028/www.scientific.net/KEM.713.14.

33. RICCIO, A., SAPUTO, S., SELLITTO, A., RAIMONDO, A. and RICCHIUTO, R. Numerical investigation of a stiffened panel subjected to low velocity impacts, *Key Engineering Materials*, 2015, **66**, pp 277-280. doi: 10.4028/www.scientific.net/KEM.665.277.

34. PIETROPAOLI, E. and RICCIO, A. Formulation and assessment of an enhanced finite element procedure for the analysis of deamination growth phenomena in composite structures, *Composite Science and Technology*, 2011, **71**, pp 836-846. doi: 10.1016/j.compscitech.2011.01.026.

35. CARRUTHERS, J., KETTLE, A. and ROBINSON, A. Energy absorption capability and crashworthiness of composite material structures: A review, *Applied Mechanics Reviews*, 1998, **51**, pp 635-649. doi: 10.1115/1.3100758.

36. JOHNSON, A. and KOHLGRUBER, D. Design and performance of energy absorbing subfloor structures in aerospace applications, *IMechE Seminar S672*, Materials and Structures for Energy Absorption, London, England, May 2000.

37. MC CARTHY, M. and WIGGENRAAD, J. Numerical investigation of a crash test of a composite helicopter subfloor structure, *Composite Structures*, 2001, **51**, pp 345-359. doi: 10.1016/S0263-8223(00)00150-1.

38. VICENTE, J.L.S., BELTRÁN, F. and MARTÍNEZ, F. Simulation of impact on composite fuselage structures, European congress on computational methods in applied sciences and engineering ECCOMAS 2000; 11-14 September 2000, ECCOMAS, Barcelona, Spain; Regensburg, Germany.

39. HANAGUD, S., CRAIG, I., SRIRAM, P. and ZHOU, W. Energy absorption behaviour of graphite epoxy composite sine webs, *J Composite Materials*, 1989, **23**, (5), pp 448-459. doi: 10.1177/002199838902300502.

40. JERYAN, R. Energy management working group activities, Proceedings of the 48th MIL-HDBK-17 Coordination Meeting-Crashworthiness Working Group, March 2005, Charlotte, North Carolina, US.

41. NAILADI, C. A summary of the ACC tube testing program, Proceedings of the 49th MIL-HDBK-17 Coordination Meeting, December 2005, Santa Monica, California, US.

42. JACKSON, A., DUTTON, S., GUNNION, A. and KELLY, D. Investigation into laminate design of open carbon-fibre/epoxy sections by quasi-static and dynamic crushing, *Composite Structures*, 2011, **93**, pp 2646-2654. doi: 10.1016/j.compstruct.2011.04.032.

43. FAUZAN, D., SHAHRUM, A., AHMAD, K.A. and ZULKIFLI, M.N. Multi objective optimization of foam-filled circular tubes for quasi-static and dynamic responses, *Latin American J Solids and Structures*, 2015, **12**, (6), pp 1126-1143. doi: 10.1590/1679-78251638.

44. REN, Y.R., JIANG, H.Y., JI, W.Y., ZHANG, H.Y., XIANG, J.W. and YUAN, F.G. Improvement of progressive damage model to predicting crashworthy composite corrugated plate, *Applied Composite Materials*, 2018, **25**, (1), 45-66. doi: 10.1007/s10443-017-9610-z.

45. JIANG, H.Y., REN, Y.R., GAO, B.H. and XIANG, J.W. Numerical investigation on links between the stacking sequence and energy absorption characteristics of fabric and unidirectional composite sinusoidal plate, *Composite Structures*, 2017, **171**, 382-402. doi: 10.1016/j.compstruct.2017.03.047.

46. BONNIE, W. and PAOLO, F. Crushing behavior of laminated composite structural elements: Experiment and LS-DYNA simulation, DOT/FAA/TC-15/25, US Department of Transportation, Federal Aviation Administration, 2016, pp 1-213.